Direct observation of Bloch harmonics and negative phase velocity in photonic crystal waveguides.

H. Gersen,[1,*] T.J. Karle,[2] R.J.P. Engelen,[1] W. Bogaerts,[3] J.P. Korterik,[1] N.F. van Hulst,[1] T.F. Krauss,[2] and L. Kuipers[1,4]

[1] *Applied Optics group, Department of Science & Technology and MESA+ Institute for Nanotechnology, University of Twente, P.O. Box 217, 7500 AE Enschede, The Netherlands.*

[2] *School of Physics and Astronomy, University of St. Andrews, St. Andrews, Fife, KY16 9SS, Scotland.*

[3] *Ghent University - IMEC, Dept. of Information Technology (INTEC), B-9000 Gent, Belgium.*

[4] *FOM-Institute for Atomic and Molecular Physics (AMOLF), Kruislaan 407, 1098 SJ Amsterdam, The Netherlands.*

(Dated: June 27, 2004)

The eigenfield distribution and band-structure of a photonic crystal waveguide (PhCW) have been measured with a phase-sensitive near-field scanning optical microscope. Bloch modes, which consist of more than one spatial frequency, are visualized in the PhCW. In the band-structure multiple Brillouin zones due to zone folding are observed in which positive and negative dispersion is seen. The negative slopes are shown to correspond to a negative phase velocity but positive group velocity. The lateral mode profile for modes separated by one reciprocal lattice vector is found to be different.

PACS numbers: 42.70.Qs, 68.37.Uv, 78.67.-n, 42.25.-p

The ability to control the flow of light in photonic crystals (PhCs) is both scientifically and practically important. Optical waves propagating in a PhC experience a spatially periodic modulation of the index of refraction and, as a result, exhibit behavior that is similar to electrons in a semiconductor crystal.[1] PhCs have the capacity of drastically affecting the optical dispersion relations, symmetries, and spatial distribution of electromagnetic modes and thereby provide a new dimension in controlling the flow of light and the construction of novel integrated optical devices.[2]

Incorporation of structural defects into PhCs allows the implementation of various functional components.[2] Arguably the most important type of defect guides in PhCs is a straight guide with one or more rows of holes missing.[3–5] Properly designed, these missing rows form a PhC waveguide (PhCW) which allows efficient guiding of light within a photonic bandgap. Due to the periodicity imposed on such a waveguide, its guided modes obey the Bloch theorem.[7, 8] This results in an intricate interplay between the guided modes and their local environment. A major practical obstacle in experimentally unravelling this interplay is the low signal levels involved combined with Fabry-Perot oscillations resulting from multiple poorly matched interfaces on the sample.[6] To understand the intricacies of light propagation in such a system and test theory, imaging the flow of light is clearly highly advantageous.

Conventional imaging of a PhCW has been found suitable for mapping the dispersion of leaky PhCW modes exploiting the interference between counter-propagating waves.[9] However, direct information concerning the field distribution of the modes being present is not obtained as the resolution of this method is intrinsically limited by diffraction. Furthermore, true guided PhCW modes have a propagation constant larger than that in air for the same optical frequency. They can therefore not be observed with far-field techniques because their field in air is evanescent, i.e. exponentially decaying over distances of the order of the light wavelength. Evanescent fields can only be detected by a local probe immersed into the near-field of the sample with a collection mode near-field optical microscope (NSOM).[10]

It has been demonstrated numerically that high-resolution NSOM images of intensity distributions can portray the path that light takes in the crystal. As a result of counter-propagating Bloch waves in finite structures, also wave-vector dispersion information can be obtained.[11] To this date several exciting NSOM experiments have been performed on PhCs, however none of which directly probe the eigenmodes of the PhC waveguide or the wave-vector dispersion diagram.[12–15]

In this Letter the local measurement of the band structure in a PhCW is demonstrated with a phase-sensitive heterodyne NSOM. Bloch modes consisting of more than one spatial frequency are measured, revealing multiple Brillouin zones due to zone folding. In addition the underlying lateral mode structure of all the PhCW modes present is determined. We find that the modal distribution for lines separated by the reciprocal lattice vector is not identical.

The majority of NSOM experiments detect local intensity distributions. However, by interfering the light collected by the optical probe with a frequency shifted reference beam from the same laser source one can obtain the local field amplitude and phase (see Fig. 1).[16–19] By detecting the interference signal with a lock-in amplifier (LIA), the X and Y quadratures of the LIA signal provide the cosine and sine of the phase difference between the NSOM light and the reference beam.[18]

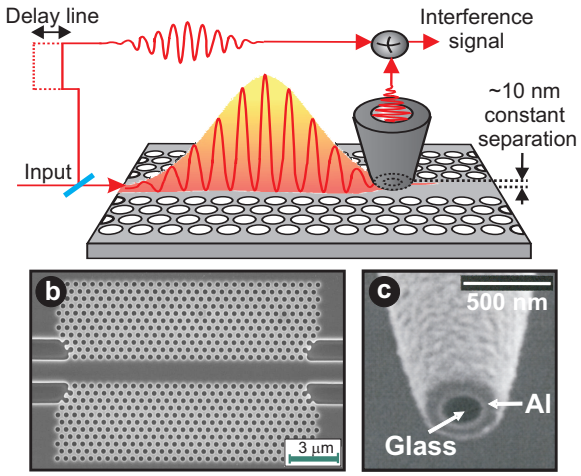

FIG. 1: (Color) Schematic representation of a phase-sensitive NSOM experiment on a W3 PhCW. The evanescent field of a pulse travelling inside the photonic structure is picked up by a coated fiber probe with a subwavelength aperture as shown in (c). At each position the signal picked up by the probe is interferometrically mixed with part of the same pulse that has propagated through the reference branch giving access to the local field amplitude and phase. (b) A scanning electron micrograph of the sample under study.

The experimental arrangement used consists of a heterodyne time-resolved collection mode NSOM as described elsewhere.[20, 21] To prevent coupling of stray light, the optical fiber tip is coated with aluminum with a focussed ion beam milled aperture of 240 nm at the end of the tip as shown in Fig. 1c.[22] By using short laser pulses as depicted in Fig. 1 the background resulting from Fabry-Perot reflections and scattering out of the structure can be completely suppressed by discrimination in the time domain. The pulses launched into the PhCW are generated by a Ti:Sapphire-pumped optical parametric oscillator (Spectra-Physics Opal). Linearly TE-polarized light (E $\parallel$ to crystal plane) with a tunable center wavelength (1180 – 1345 nm) is coupled to the PhCW.

The structure under investigation is a W3 PhCW fabricated in a Silicon-on-Insulator (SOI) wafer, comprising a 220 nm Si core on top of a 1 μm SiO_2 cladding. The patterns were defined by Deep UV 248 nm lithography.[23] Holes are arranged in a hexagonal array (period $a = 460$, hole radius $r = 130$ nm) and three rows of missing holes define the so-called W3 PhCW along the ΓK direction of the irreducible Brillouin zone of the lattice. This resulted in the structure shown in Fig. 1b. The PhCW displayed in Fig. 1b. is significantly shorter than the one used in the NSOM measurements (32 versus 256 crystal periods), but allows all the relevant features of the structure to be seen in detail.

The result of a local phase-sensitive heterodyne interference measurement on a W3 PhCW is shown in Fig. 1. Fig. 2a shows the measured topography (image size: 126.0 μm×8.1 μm), which is collected simultaneously with the optical information. The access and exit waveguide are visible at the left and right side of the image and the hexagonal hole pattern that forms the PhC can also be recognized. Fig. 2b shows the raw data of one of the LIA signals, which corresponds to the local optical amplitude times the cosine of the phase[21]. In the PhCW guided light with a large spread in spatial frequencies is visible. From the two LIA signals the optical amplitude can be separated (depicted in Fig. 2c). It is apparent that pulses with different modal distributions are excited in the PhCW. The pulses are clearly separated after only a short propagation length, a clear indication of the strong dispersive properties of the PhCW. The dominant periodicity observed in Fig. 2c corresponds to 460 nm as expected for Bloch modes in periodic media with that period.[24, 25]

A spatial Fourier-transform (SFT) of the raw LIA data as displayed in Fig. 2b directly reveals what spatial frequencies are present in the measurement as well as their relative amplitudes.[18] The measurements and subsequent Fourier analysis are repeated for different wavelengths ranging from 1180 to 1345 nm in steps of 5 nm. To improve signal to noise all individual scan lines on the PhCW itself are summed after the SFT operation. Figure 3a shows the band structure constructed from the measured spatial frequencies. The vertical axis displays the excitation wavelength in terms of the normalized frequency (ω), while the horizontal axis corresponds to the observed spatial frequencies in terms of the normalized wave vector (k). To enhance the dynamic range of the displayed measured intensities a logarithmic color scale is applied. Modes both above and below the light-cone (dotted line) are detected. Our local measurement technique reveals zone folding as multiple Brillouin zones (BZ) are observed.

In addition to probing the band structure of the PhCW modes, the use of a phase-sensitive NSOM allows the determination of the underlying mode structure of all the the PhCW modes present. The lateral field profile of a mode is obtained by determining the amplitude of the peak in the SFT spectrum, corresponding to that mode, as function of the direction perpendicular to the propagation direction.[17, 18] By displaying the amplitude of SFT for each individual scan line of Fig. 2b along the waveguide the field profile can be displayed for all modes at the same time. The result of this Fourier analysis for $\omega = 0.369$ as presented in Fig. 2b is displayed in Fig. 3b. Each horizontal line corresponds to the SFT of a horizontal line from Fig. 2b on a linear scale. Values between $k = 1 - 2$ are multiplied by 5 to enhance visibility of weak modes in the 2nd BZ. A vertical line for a certain spatial frequency thus corresponds to the lateral mode profile for that specific mode. As a result Fig. 3b directly displays the modal distribution of all PhCW modes for $\omega = 0.369$. For reference the topography displayed in Fig. 2a should

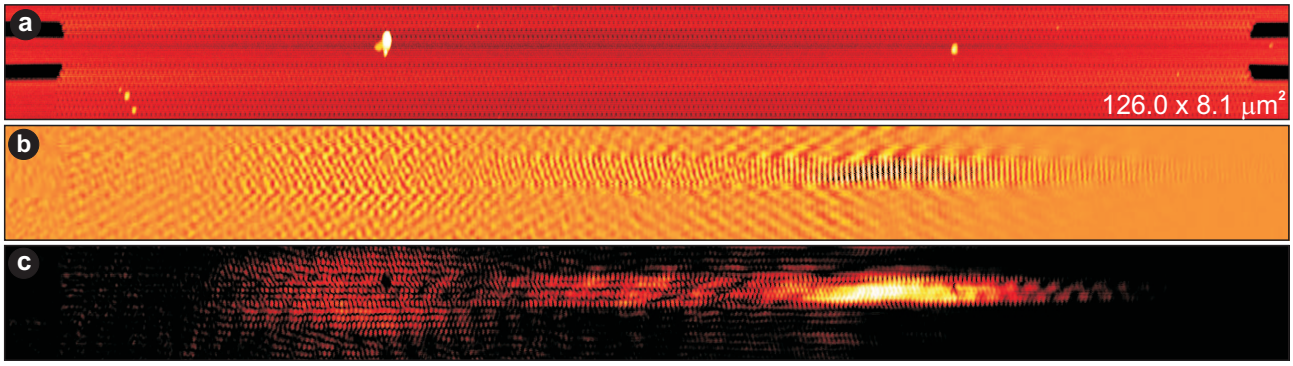

FIG. 2: (Color) A phase-sensitive NSOM measurement on a W3 PhC waveguide for a fixed position of the optical delay (image size: 126.0 μm×8.1 μm). Short pulses (FWHM 123 fs, TE-polarized) were launched in the access waveguide at a wavelength of 1245 ± 0.5 nm ($\omega = 0.369$ for $a = 460$ nm). (a) Topographic image of the structure. (b) False color images of the raw data from the lock-in amplifier corresponding to the amplitude times the cosine of the optical field. In the waveguide guided light with a large spread in spatial frequencies is visible. (c) The optical field amplitude as derived from (b). It is apparent that pulses with different modal distributions are excited in the W3 waveguide. The dominant periodicity observed in (c) corresponds to 460 nm as expected for Bloch modes.

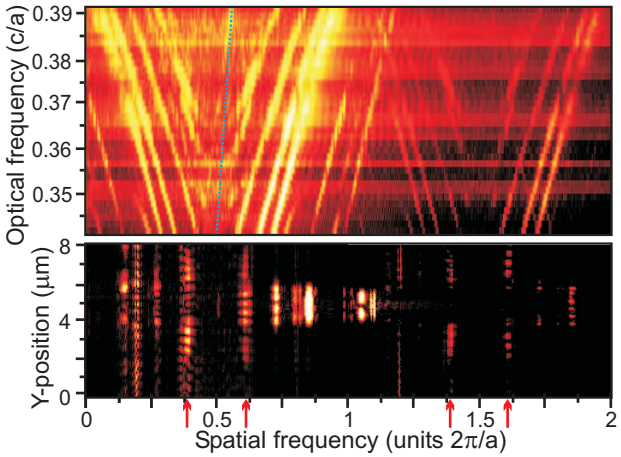

FIG. 3: (Color) (a) Experimentally mapped dispersion diagram of the modes excited in the W3 waveguide. Displayed is the Fourier transform of the raw data for multiple excitation wavelengths on a logarithmic scale. A summation has been performed over scan lines on the PhCW for each individual wavelength. Clearly modes below and above the light-cone (dotted line) are visible. (b) Displays the lateral mode distribution for $\omega = 0.369$ by displaying the SFT from each individual scan line on a linear scale. To enhance the visibility of weak modes in the 2nd Brillouin zone values between $k = 1$ – 2 are multiplied by 5. Here we can directly see the modal distribution for each of the lines in the dispersion diagram at $\omega = 0.369$. It is clear that for Bloch harmonics that belong to the same Bloch mode, e.g. indicated by arrows, the modal distribution is not the same.

be used. Both modal distributions that are completely confined to the waveguide regions and with significant field tails in the PhC are observed.

Bloch modes contain more than one spatial Fourier component. These Bloch harmonics are separated by $2\pi/a$, where a is the periodicity. This separation is obvious in Fig. 3a where we displayed the first two Brillouin zones. An example of Bloch harmonics that belong to the same Bloch mode for $\omega = 0.369$ are indicated by the arrows in Fig. 3b and 4a. Here Fig. 4a depicts the SFT of the data for $\omega = 0.369$ on a logarithmic scale. In literature lines separated by an integer number of reciprocal lattice vectors are often considered to be identical. However, if we look in Fig. 3b at the mode patterns for the wave vectors 0.60 and 1.60 we immediately see that the modes patterns are not the same. For the indicated Bloch harmonics (see arrows) the line traces as shown in Fig. 4b demonstrate that the mode profile differs for all of them. In Fig. 3b this effect is also visible for the Bloch harmonics of other Bloch modes. It is clear that the modal distributions for Bloch harmonics separated by $2\pi/a$ is different.

In one Brillouin zone in Fig. 3a lines with both negative and positive slope are visible as a result of zone folding. For the Bloch harmonics at $k = 0.393$ and $k = 0.607$, the cosine and sine signal from the LIA are shown in the top and bottom panel of Fig. 4c, respectively. This data is retrieved by an inverse Fourier transform after applying a Gaussian filter centered on the desired peak. It is clear that in the top panel($k = 0.393$) the sine is in front, while in the bottom panel($k = 0.607$) the sine is lagging. As the LIA signal provides the cosine and sine of the phase difference between the NSOM light and the reference light simple goniometry shows that the wave vectors for the two Bloch harmonics have an opposite sign. It is interesting to observe that the energy of the Bloch mode propagates in a direction opposite to the k-vector for one of these modes.[26] Because this mode is referenced by this k-vector, the group velocity is negative in a formal way and hence appears as a negative slope. However, advancing the optical delay such that the reference pulse

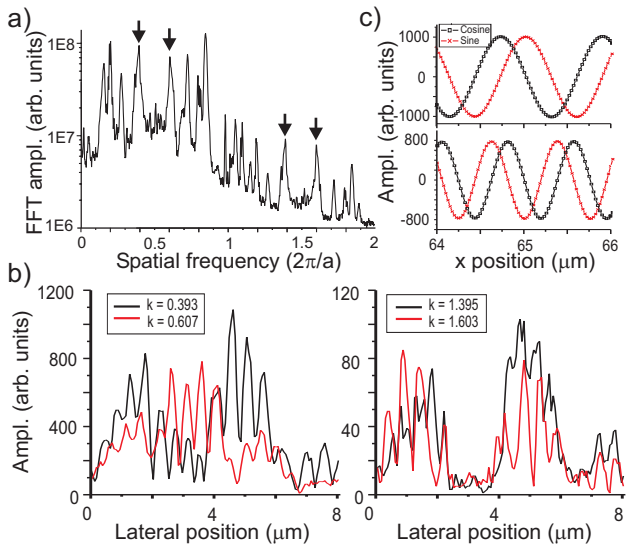

FIG. 4: (Color) (a) Spatial Fourier transform for $\omega = 0.369$ with all scan lines on the PhCW summed. Arrows indicate peaks that belong to the same Bloch mode. (b) Lateral mode profiles for the Bloch harmonics indicated by the arrows in Fig. 3b and Fig. 4a. Clearly the modal distribution is different for each individual Bloch harmonic. (c) A Fourier filter allows retrieval of the phase evolution of individual modes. Top panel in (c) shows the sine and cosine channel of the LIA for $k = 0.393$, while bottom panel corresponds to $k = 0.607$. For the Bloch harmonic at $k = 0.393$ the sine is in front, while it is lagging at $k = 0.607$. As a result the wave vectors for these two harmonics from the same Bloch mode have an opposite sign.

travels a longer distance directly proves that the pulses advance along the PhCW, i.e., in the positive direction. From the experimental data it is therefore obvious that these modes have a positive group velocity and a negative phase velocity.

In conclusion, we have measured multiple Brillouin zones in a W3 photonic crystal waveguide. Lines with both positive and negative slope are observed in one Brillouin zone. We demonstrated that modes with a negative slope have a positive group velocity and a negative phase velocity. Furthermore, for each individual mode observed in the band structure we retrieved the modal distribution. Comparison of wave vectors separated by the reciprocal lattice constant demonstrates that the modal distribution is different for individual Bloch harmonics. It is envisioned that this demonstration of probing both the eigenfield distribution and the band-structure information of a photonic crystal waveguide (PhCW) and the determination of the relative sign of wave-vector and the group velocity will open up further experimentation in areas such as optical Bloch oscillations[28], quasicrystals[27], negative refraction and left-handed behavior[29] and many others.

This research is part of the strategic Research Orientation on Advanced Photonic Structures of the MESA$^+$ Institute for Nanotechnology. Furthermore, this work is part of the research programme of the Stichting voor Fundamenteel Onderzoek der Materie (FOM), financially supported by the Nederlandse Organisatie voor Wetenschappelijk Onderzoek(NWO). Wim Bogaerts is supported by the European Union as part of the IST-PICCO project. Tim Karle acknowledges support by a CASE award from Agilent Technologies.

* corresponding author : h.gersen@alumnus.utwente.nl

[1] J.D. Joannopoulos, R.D. Meade, and J.N. Winn, *Photonic crystals : Molding the flow of light* (Princeton University Press, Princeton NY, 1995).
[2] See for example, *Photonic Crystals and Light Localization in the 21st Century,* in *NATO Science Series,* C.M. Soukoulis, ed. (Kluwer Academic, Dordrecht, The Netherlands, 2001).
[3] H. Benisty, J. Appl. Phys. **79,** 7483 (1996).
[4] T.F. Krauss, R.M. De La Rue, and S. Brand, Nature **383,** 699 (1996).
[5] S.G. Johnson, *et al.*, Phys. Rev. B **62,** 8212 (2000).
[6] S. J. McNab, N. Moll, and Y. A. Vlasov, Opt. Expr. **11,** 2927 (2003).
[7] S. Olivier, *et al.*, Phys. Rev. B **63,** 113311 (2001).
[8] M. Agio, and C.M. Soukoulis, Phys. Rev. E **64,** 055603 (2001).
[9] M. Lončar, *et al.*, Appl. Phys. Lett. **80,** 1689 (2002).
[10] For a recent review, see V. Sandoghdar, *et al*, in *Photonic crystals : advances in design, fabrication, and characterization* (Wiley-VCH, Weinheim, Germany, 2004).
[11] S. Fan, I. Appelbaum, and J.D. Joannopoulos, Appl. Phys. Lett. **75,** 3461 (1999).
[12] S.I. Bozhevolnyi, *et al.*, Phys. Rev. B **66,** 235204 (2002).
[13] E. Flück, *et al.*, Phys. Rev. E **68,** 015601 (2003).
[14] K. Okamoto, *et al.*, Appl. Phys. Lett. **82,** 1676 (2003).
[15] P. Kramper, *et al.*, Phys. Rev. Lett. **92,** 113903 (2004).
[16] M. Vaez-Iravani, and R. Toledo-Crow, Appl. Phys. Lett. **62,** 1044 (1992).
[17] M.L.M. Balistreri, *et al.*, Phys. Rev. Lett. **85,** 294 (2000).
[18] M.L.M. Balistreri, *et al.*, J. Lightwave Technol. **19,** 1169 (2001).
[19] A. Nesci, *et al.*, Opt. Comm. **205,** 229 (2002).
[20] M.L.M. Balistreri, H. Gersen, *et al.*, Science **294,** 1080 (2001).
[21] H. Gersen, *et al.*, Phys. Rev. E **68,** 026604 (2003).
[22] J.A. Veerman, *et al.*, Appl. Phys. Lett. **72,** 3115 (1998).
[23] W. Bogaerts, *et al.*, Opt. Expr. **12,** 1583 (2004).
[24] P. St. J. Russell, Appl. Phys. B **39,** 231 (1986).
[25] P. St. J. Russell, J. of Modern Optics, **38,** 1599 (1991).
[26] J. Witzens, M. Lončar, and A. Scherer, IEEE J. Select. Topics. Quantum Electron. **8,** 1246 (2002).
[27] L. Dal Negro, *et al.* Phys. Rev. Lett. **90,** 055501 (2003).
[28] R. Sapienza, *et al.* Phys. Rev. Lett. **91,** 263902 (2003).
[29] S. Foteinopoulou and C.M. Soukoulis, Phys. Rev. B **67,** 235107 (2003).